ADVANCED OPTICAL MATERIALS
www.advopticalmat.de

Liquid Crystals for Superior Electro-Optic Performance Display Device with Power-Saving Mode

MinSu Kim, Heui Seok Jin, Seung Jae Lee, Yun-Ho Shin, Hyeong Gyun Ham, Deng-Ke Yang, Philip J. Bos, Joong Hee Lee, and Seung Hee Lee**

An advantageous factor for the technology of displays is low power consumption. For power-saving, low-frequency driving of liquid crystal displays (LCDs) is useful. However, an unacceptable performance drop, from image-flickering, occurs due to occurrence of the flexoelectric effect. Here, based on close agreement between experimental and simulated results, a new electro-optic mode with optimization of both electrode structures and physical properties of the liquid crystal materials is demonstrated. Although the calculated electro-optic properties are obtained for particular simulation conditions, the achieved transmittance is exceptional for LCDs using a power-saving mode, and can result in complete elimination of static and dynamic flickering. It is believed the result will pave the way toward successful design for low-power consumption and high-performance LCDs.

1. Introduction

Lowering global energy consumption is being pursued as a long-term plan by global energy agencies.[1] Electronic and electric devices consume large amount of energy in daily life, so the efforts to improve the device performance should be accompanied with the efforts to reduce the power consumption as well. For this reason, and related to the limited capability of battery for portable devices, it is required to find a way to lower the power consumption as much as possible.

The power consumption of liquid crystal displays (LCDs) significantly depends on its backlight unit, so reducing power consumption of the backlight is an important task to pursue in LCDs using approaches such as dynamic backlight dimming.[2,3] Besides the effort related to the backlight unit, one can still look for the additional power reduction in the liquid crystal driving scheme, for example, by reducing the driving frequency *f*. Displaying smooth and dynamic motion at high-frame rate has been an unquestionable direction to improve the performance of displays, but static images are also becoming significantly important as the application of displays diverges. Thus, as the *f* is in linear dependence on the power consumption of a module, low-*f* driving LCD is desired.

In driving scheme of LCDs, some amount of electromagnetic radiant energy from the backlight is cut off by the combination of crossed polarizers and liquid crystalline medium while modulating polarization. In terms of energy loss in a liquid crystal layer, therefore, maximizing transmittance is an important factor to improve for better electro-optic performance. From this perspective, achieving both high optical transmittance and low-*f* driving would be a remarkable breakthrough in terms of power savings.

There are two main streams of the initially homogeneous aligned light modulating mode in LCDs: fringe-field switching (FFS) and in-plane switching (IPS) modes. Both modes have a patterned electrode on the one side of two sandwiched substrates. In the IPS mode, patterned pixel (signal-swung) and common electrodes are interdigitated such that symmetrical lateral fields, which have the same translational periodicity with the electrode patterns, are formed between these two electrodes to rotating the liquid crystal director in plane; thus, reorientation occurs only in between the electrodes. In the FFS mode, on the other hand, a plain common electrode and a patterned pixel electrode are not on the same layer and separated by an insulation layer. With this structure, the electric fields form nonsymmetrical fringe shape and the field periodicity is half of the pitch of the electrode patterns. Thus, the rotation of the liquid crystal director takes place over the entire electrode area, which contributes more to the optical transmittance.[4,5]

The FFS mode has been dominating the LCD market, especially in portable devices owing to the high aperture ratio, high transmittance, low operation voltage, wide-viewing angle, and touchscreen tolerance.[4,6] Consequently, intensive efforts to reduce the power consumption of this mode have been attempted by using the low-*f* driving when static images are being displayed. However, severe issues regarding image quality arise in the low-*f* driving, including image-flickering owing to flexoelectric effect.[7–14] The flexoelectric effect is a

Dr. M. S. Kim,[+] H. S. Jin, S. J. Lee, H. G. Ham, Prof. J. H. Lee, Prof. S. H. Lee
Department of BIN Convergence Technology
Applied Materials Institute for BIN Convergence
and Department of Polymer Nano-Science and Technology
Chonbuk National University
Jeonju, Jeonbuk 561-756, Korea
E-mail: mkim182@jhu.edu; lsh1@chonbuk.ac.kr
Dr. M. S. Kim, Y.-H. Shin, Prof. D.-K. Yang, Prof. P. J. Bos
Liquid Crystal Institute
Kent State University
Kent, OH 44242, USA
The ORCID identification number(s) for the author(s) of this article can be found under https://doi.org/10.1002/adom.201800022.
[+]Present address: Department of Physics and Astronomy, Johns Hopkins University, Baltimore, MD 21218, USA

DOI: 10.1002/adom.201800022

coupling between elastic deformation and electric polarization of liquid crystals in which the flexoelectric polarization is spontaneously induced by external electric field at a low *f*.[15–19] This effect has been known to occur with high-flexoelectric constant materials, such as a bent-core liquid crystal;[20] however, recent reports clearly show that the optical appearance of the flexoelectric effect becomes quite obvious even in rod-like nematic liquid crystal with relatively small flexoelectric coefficients, e_s (splay) and e_b (bend) <15 pC m^{-1} while horizontal electric field is applied.[19,21,22]

When the flexoelectric effect is present (flexoelectric mode), the electrode-position-dependent local transmittance has a different periodicity than without flexoelectric effect (normal mode). As the drive polarity changes, the local light transmitted area is shifted from the area in between pixel electrodes to the area above these electrodes. This effect is related to a coupling between the distorted director field resulting from applied electric fields and the flexoelectric polarization in *constructive* and *destructive* relations.[19,22]

In the IPS mode with the flexoelectric effect, the integrated brightness between positive (+) and negative (–) signal frames is the same in theory because the formation of electric fields is mirror-symmetric between frames unless the electrode width w of a pixel electrode w_p and a common electrode w_c are of different length. Thus, in this system with $w = w_p = w_c$ and a constant electrode space l, there is no *static* image-flickering, which is determined by the brightness difference between electric signal frames. However, there is a *dynamic* image-flickering that appears as an optical spike in time-dependent transmittance curves, so-called, optical bounce at the frame-transition moment.[19,22] On the other hand, although the main advantage of the FFS mode is the highest optical transmittance characteristic among all high-resolution LCD modes, both the dynamic flickering and static flickering exist because $w = w_p \neq w_c$.[4] From this perspective, the FFS mode is less advantageous in power-saving low-*f* driving mode than the IPS mode.[22] However, a recent report demonstrates the static flickering can be solved by field symmetrization by optimization of electrode structures.[21]

Detailed analysis of the optical spikes (transmittance jumping up at the frame-transition moment), which causes the dynamic image-flickering, shows that there is an abrupt change in tilt deformation of director fields in which the opposite sign of the electric field is applied while flexoelectric effect occurs. More precisely speaking, the optical spike takes place because the director tilt deformation is momentarily suppressed.[19,22]

Here, we propose to utilize this phenomenon such that the overall transmittance highly increases by keeping this momentary high transmittance for the whole frame time. Our results show a power-saving low-*f* driving FFS mode with superior electro-optic performance that keeps record-breaking transmittance with no static and dynamic image-flickering. To realize this, we demonstrate three strategies: using (1) fine-patterned pixel electrodes with negative dielectric anisotropy liquid crystals (nLC, $\Delta\varepsilon < 0$), (2) high magnitude of dielectric anisotropy $|\Delta\varepsilon|$, and (3) low-flexoelectric coefficients (e_s and $e_b < 5$). In regards to the strategy (1), nLC has been known to improve the optical transmittance in FFS mode,[23] and a fine-patterned electrode (both w and $l < 3$ μm) gives rise to highly strengthened electric fields to drive liquid crystals, thereby enhancing transmittance.[23,24] The tilt angle of liquid crystal directors with respect to an applied electric field is lower when using nLC than that using positive $\Delta\varepsilon$ (pLC), so that one can expect the splay and bend deformations become less, giving rise to mainly twist deformation of LC directors rather than tilt. With strategy (2), the suppression of tilt deformation results in higher transmittance in which the overall transmittance can be significantly enhanced as high as the transmittance at the optical spike. Finally, with strategy (3), it is unquestionable that the flexoelectric effect will be suppressed with low e_s and e_b; however, because both the flexoelectric coefficients and $|\Delta\varepsilon|$ are proportional to dipole moment, it is quite intuitive that both $|\Delta\varepsilon|$ and flexoelectric coefficients increase as the dipole moment increases. In our approach, we propose to adjust the fraction of liquid crystal molecules with different rigidity. When the molecular rigidity becomes low, the flexoelectric coefficients can be reduced and the dipole moment can still be kept high. With this material engineering approach, we propose a new way to have nLC mixtures exhibiting their e_s and e_b go low while their $|\Delta\varepsilon|$ goes high. Thus, it enables us to suppress flexoelectric effect significantly while maximizing transmittance.

2. Results

2.1. Liquid Crystal Mixtures

To promote the highest performance of liquid crystal mixtures for the low-*f* power-saving LCD mode, we used three different liquid crystal mixtures: nLC1, nLC2, and nLC3 with negative dielectric anisotropy $\Delta\varepsilon_1$, $\Delta\varepsilon_2$, and $\Delta\varepsilon_3$, respectively ($|\Delta\varepsilon_1| < |\Delta\varepsilon_2| < |\Delta\varepsilon_3|$, see **Table 1**). These contain mainly, but are not

Table 1. Physical properties of liquid crystal mixtures and cell condition in experiments.

	Δn[a)]	$\Delta\varepsilon$[b)]	γ_1[c)] [mPa s]	K_{33}/K_{11}[d)]	w[e)] [μm]	l[f)] [μm]	d[g)] [μm]	α[h)] [°]	Compound no.[i),j)]
pLC[k)]	0.0804	+5.9	193	1.46	3	4	4.5	10	–
nLC1[l)]	0.1085	**–2.1**	90	1.11	3.5	6	3.3	80	**2** > **3** > **1**
nLC2	0.1086	**–3.0**	110	1.10	3.5	6	3.3	80	**2** > **1** ≥ **3**
nLC3	0.1086	**–4.0**	140	1.08	3.5	6	3.3	80	**1** ≥ **2**

[a)]Birefringence; [b)]Dielectric anisotropy; [c)]Rotational viscosity; [d)]Ratio of bend (K_{33}) to splay (K_{11}) elastic constant; [e)]Electrode width; [f)]Space between electrodes; [g)]Cell gap; [h)]Rubbing angle with respect to horizontal field direction; [i)]The number of compounds that are contained in liquid crystal mixtures (see Figure 1); [j)]The mixtures may contain more of other compounds, which are not introduced here; [k)]Liquid crystal mixture with positive $\Delta\varepsilon$; [l)]nLC: liquid crystal mixture with negative $\Delta\varepsilon$.

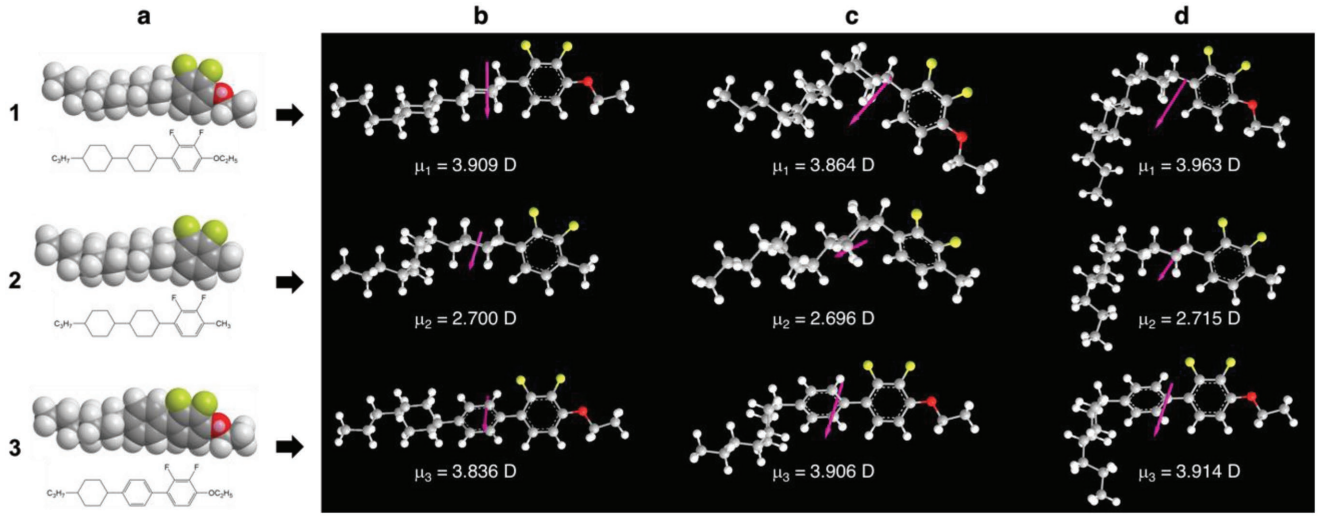

Figure 1. Single compounds in liquid crystal mixtures. a) Molecular structures: red, yellow, gray, and white indicate oxygen, fluorine, carbon, and hydrogen atoms, respectively. Calculated dipole moments with the energy minimization using MOPAC package[26] (The pink arrows indicate the dipole moment), and three possible conformations, which represent from b) straight, c) moderate, and d) bent shapes of the compounds **1**, **2**, and **3**.

limited to, three different types of compounds (**Figure 1**a). The molecular dipole moment μ was calculated at minimized energy by MOPAC package:[25] $\mu_1 \approx \mu_3 > \mu_2$, and each compound can have various conformations calculated: from straight to bent (Figure 1b–d). Also, mesoscale physical properties of the compounds are shown in **Table 2**.[26]

There is an oxygen atom attached to a benzene ring of compound **1** and **3**; thus, μ_1 and $\mu_3 > \mu_2$. The compound **3** can be expected to be more rigid, as it has a benzene ring instead of cyclohexane in the middle unlike the compounds **1** and **2**.

2.2. Suppression of Flexoelectric Effect: Magnitude of Dielectric Anisotropy versus Flexoelectric Coefficients

From a perspective of liquid crystal material engineering, our approach for high-performance low-*f* power-saving LCD mode is to design high $|\Delta\varepsilon|$ and low e_s (e_b) of mixtures based on the combination of molecular scale structural analysis and statistical approach. On the one hand, $\Delta\varepsilon$ can be controlled by adjusting the fraction of the constituents that have various dipole moments in mixtures. On the other hand, the e_s (e_b) can be engineered by balancing between the dipole moments and molecular packing. The maximized molecular packing statistics result in a precise expression of $e_s = \beta(2\mu_{\parallel}K_{11}/k_BT)N^{1/3}(a/b)^{1/3}$ and $e_b = \beta(\mu_{\perp}K_{33}/2k_BT)N^{1/3}(b/a)^{2/3}$, where $\mu_{\perp}(\mu_{\parallel})$ is dipole moment perpendicular (parallel) to the long axis of a molecule; k_BT is the thermal energy; N is the molecular number density; β and a/b (b/a) are a kink angle and the aspect ratio of molecular anisotropy, respectively.[16,18] (The molecular packing as well as N are related to the molecular rigidity.) The N can become low as the molecules in a mixture become more flexible, for example, the N of a mixture with the high fraction of compound **1**, **2** will be lower than that with the high fraction of compound **3** (again, because of the absence of one benzene ring in the middle). This effect can be independent of the magnitude of dipole moments. Thus, assuming a mixture contains molecules with high dipole moment and low rigidity, $\Delta\varepsilon$ can be kept higher while e_s (e_b) becomes lower. For instance, nLC1 contains fraction of compounds **2** > **3** > **1**, while nLC3 contains **1** > **2** without **3** (Table 1). The higher N owing to compound **3** in nLC1 leads to higher e_s (e_b).[18,27] Consequently, nLC3 can have higher $|\Delta\varepsilon|$ but lower e_s (e_b) than nLC1. In this way, the flexoelectric effect can be very efficiently suppressed owing to not only high $|\Delta\varepsilon|$ but also low e_s (e_b). (See the Discussion for more details with Figure S1 and Table S1, Supporting Information.)

Table 2. Mesoscale physical properties of the single compounds.[26]

No.	Δn	$\Delta\varepsilon$	γ_1 [mPa s]
1	0.096	−5.9	413
2	0.095	−2.7	218
3	0.156	−5.9	233

2.3. Simulation Condition for Liquid Crystal Director Field and Optical Transmittance

A numerical simulation was done by a commercialized multidimensional finite element method (FEM) solver (TechWiz LCD, SANAYI System Co., Ltd.). The flexoelectric effect as well as flexoelectric polarization can be described as $P_f = e_s \boldsymbol{n}(\nabla \cdot \boldsymbol{n}) + e_b \boldsymbol{n} \times (\nabla \times \boldsymbol{n})$, where n is a director that represents orientation of liquid crystal molecules. The head-tail symmetry of nematic liquid crystal is broken because liquid crystal directors are able to follow the polarity of an electric signal in a single signal frame. Such a system can be described by free energetic terms: the elastic free energy density $f_{elas} = \frac{1}{2}\left(K_{11}[\nabla \cdot \boldsymbol{n}]^2 + K_{22}[\mathbf{n} \cdot (\nabla \times \boldsymbol{n})]^2 + K_{33}[\mathbf{n} \times (\nabla \times \boldsymbol{n})]^2\right)$, the quadratic dielectric coupling $f_{dielec} = -\frac{1}{2}\varepsilon_0 \Delta\varepsilon(\boldsymbol{n} \cdot \boldsymbol{E})^2$, and the linear flexoelectric coupling $f_{flexo} = -\boldsymbol{P}_f \cdot \boldsymbol{E}$, where K_{11}, K_{22}, and K_{33} are splay, twist, and bend elastic constants of liquid crystals; ε_0 and E are dielectric constant in a vacuum and an

external electric field, respectively. The distribution of electric potential was calculated by Laplace's equation, and optical images, for comparing to the POM images, were generated based on the [2 × 2] extended Jones matrix method.

The flexoelectric coefficients were set to e_s (e_b) = 0 (0) pC m^{-1} for the normal mode, and the ratio e_s/e_b = 0.5 for nLCs. It can be quite reasonable to consider averaging out two possible conformations for nematic liquid crystals:[18,27,28] (1) an elongated shape with mostly *trans* conformation, $e_s/e_b \sim 1$; (2) the most bent shape with a single *gauche* link in terminal chain, $e_s/e_b = 0.2$ (see Figure 1b,d). Adjustment of $\Delta\varepsilon$ and rotational viscosity γ_1 of liquid crystals is extrapolated by following the linear correlation between $\Delta\varepsilon$ and γ_1.[29] While adjusting $\Delta\varepsilon$ and γ_1, the other liquid crystal properties were set to be the same, such as mechanical (elastic constants) and optical properties (refractive indices).

2.4. Flexoelectric Effect in Experiment and Simulation with pLC

To investigate the flexoelectric effect in nematic liquid crystals experimentally, a FFS cell was prepared. A cross-sectional view of electrode structure is schematically illustrated in **Figure 2**a and the voltage-on state of polarizing optical microscopy (POM) images is shown in Figure 2b. One glass substrate side has a stack of three layers: from the bottom, a plane electrode of a transparent indium-tin-oxide (ITO) layer (for constant voltage), an insulation layer h, and a zig-zag electrode of the other ITO layer that was patterned by photolithography with w (l) = 3 (4) µm to apply the signal voltage.

The optical appearance of flexoelectric effect in nematic liquid crystal is compared in Figure 2a,b. The optical brightness is spatially shifted in Figure 2a and the optical appearance of the flexoelectric effect is more clearly observed at the borderline between domains in the zig-zag electrode in Figure 2b. (The domain here is determined by the same electrode direction.) The experiment and simulation are in quite close agreement with each other as can be seen in the enlarged POM and 2D FEM images. Interestingly, unlike in (+) frame, the dark area at the borderline becomes sawtooth-shaped in (–) frame. The overall integrated transmittance behavior is measured as the time-dependent transmittance curves in Figure 2c. The T_{pom} is spatial average of pixel brightness in POM images and EO denotes electro-optic measurement by the light source and the photodetector. Here, the other interesting point is that the optical bounce is only observed in the transition from (–) to (+) frame, but not from (+) to (–) frame. It is necessary to identify the difference between the (+) and (–) frames because not only the two-domain patterned electrode structure is quite common in commercialized LCDs for improving viewing-angle property in off-normal angles but also potential distribution near the area at the domain borderline can be different from the area along linear electrodes. To understand the reasons, POM images were acquired every 10 ms and 3D FEM images are compared with them.

2.5. Detailed Analysis of Flexoelectric Effect in Zig-Zag Electrodes with pLC

One-domain simulation can be done with 2D solver but two-domain simulation requires 3D solver with proper decision of boundaries. For FEM calculation, we first drew the common electrode (com), insulation layer (insul), and signal electrode (sig), and then decide the simulation area (sim) with periodic boundaries in both horizontal and vertical axes (see Figure S3, Supporting Information). The horizontal boundary was decided to have the same length scale as the experimental electrode value. To reduce the running time, the vertical boundary was chosen to be less than the distance in the experiment, but we

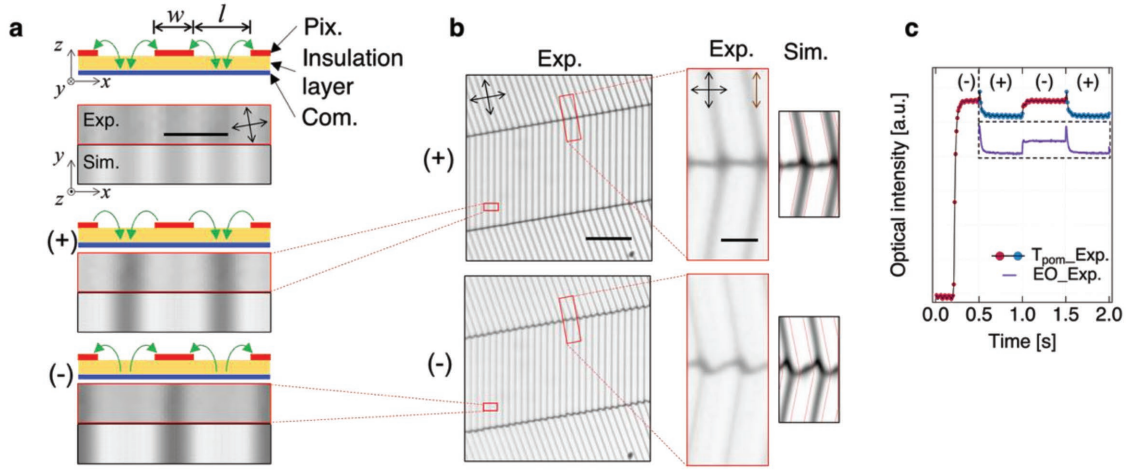

Figure 2. Appearance of flexoelectric effect in a uniformly aligned nematic liquid crystal driven by FFS mode. a) Schematics of cross-sectional electrode structure with electric field formation (green arrows). POM images and 2D FEM images at normal mode and flexoelectric mode in (+) and (–) signal frames. Scale bar is 5 µm. b) POM images driven at f = 1 Hz at 6.2 V_{pp} (50% of maximum transmittance) with zig-zag electrodes. (Here, a domain is determined by the same electrode direction.) Enlarged POM images are compared to 3D FEM simulated images. Black and brown arrows indicate crossed polarizers and initial direction of directors, respectively. Scale bars are 50 µm, and 4 µm in enlarged images. c) Measured time-dependent transmittance at f = 1 Hz. The T_{pom} means spatial average of pixel brightness in POM images and EO denotes electro-optic measurement by the photodetector.

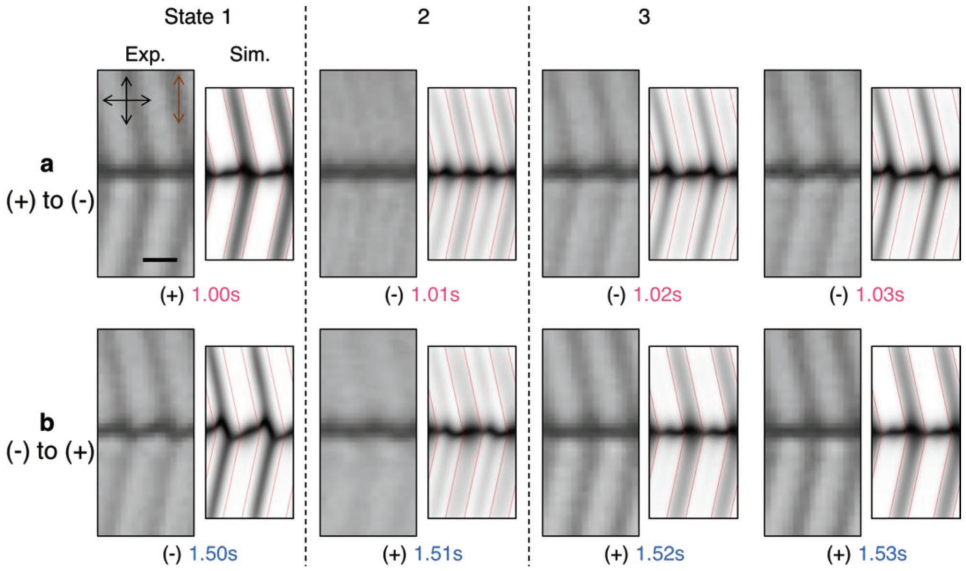

Figure 3. POM and 3D FEM images at the frame-transition moments. a) (+) to (–) and b) (–) to (+) frame transitions. Black and brown arrows indicate crossed polarizers and initial direction of directors, respectively. Scale bar is 4 μm. (See Movies S1–S4, Supporting Information, for dynamic POM observation at f = 60, 30, 10, and 1 Hz, respectively.)

ensured enough distance between edges so the director field in the middle area of the electrode would not be affected by the director field near the edge.

In **Figure 3**, the images are shown at the frame-transition moment from (+) to (–) frame or vice versa with the same time scale in Figure 2c. The observation informs that, (1) the dark area seems wider in (+) frame than that in (–) frame as one may specifically notice in the State 1 of Figure 3 as well as in Figure 2b, which can be one of the reasons that the spatially integrated transmittance in (–) frame is higher than that in (+) frame; (2) the sawtooth-like domain boundary is apparent in (–) frame (State 1 of Figure 3b) and disappears at the moment of an opposite frame applied (State 2 of Figure 3b); (3) the vertical dark area momentarily disappears upon the opposite frame applied (State 2) and then the bright area shifted to the other side of the electrode (from State 1 to 3). Based on the results, one could deduce two facts: (1) the flexoelectric coefficients used in simulation seem reasonable; (2) detailed analysis of the simulation result can tell us the reason of the different optical bounce appearing at frame transitions and how the sawtooth-shaped borderline matters in this phenomenon.

For the analysis on the appearance of the sawtooth-shaped borderline, on the one hand, we look back to the cross-sectional view of the schematics shown in Figure 2a. The field-potential becomes asymmetric between (+) and (–) frames owing to the insulation layer between pixel and common electrodes.[21] In (+) frame, the order of elements in the circuit is: (1) electrode, (2) liquid crystal, (3) insulation layer, (4) electrode, whereas in (–) frame, it is (1) electrode, (2) insulation layer, (3) liquid crystal, (4) electrode. In addition to this insulation layer effect, one should take the fact into account that the potential distribution becoming complicated at the domain boundary, and should also pay attention to the difference between frames for both the electric potential distribution and the director field at this boundary (**Figure 4**). The gradient of the electric potential distribution becomes relatively complicated near the domain boundary (as the electric field indicated by the black solid arrows at z = 0 μm in Figure 4a,c). This field gradient basically gives rise to multiple azimuthal-directional flexoelectric polarization so that flexoelectric coupling occurs at this area, three-dimensionally. At z = 2 μm, both region A (the area on a common electrode in (–) frame) and B (a pixel electrode in (+) frame) are at higher potential than each of the counter-electrodes. The aspect of the potential distribution in the region A and B along the long direction of the electrode is different, that is, B is relatively more uniform than A. Thus, assuming there is a mirror plane at the domain boundary along the black dotted arrows (Figure 4a,c), the potential distribution between domains is relatively more mirror symmetric in (+) frame (Figure 4a) than that in (–) frame (Figure 4c). This reveals the reason of the sawtooth-shaped border lines in the (–) frame.

On the other hand, for the analysis on the occurrence of the different optical bounce between frames, we remember the fact that one of the main reasons for an optical bounce is the tilt deformation associated with *constructive* flexoelectric coupling.[22] Such tilt deformation (region D in Figure 4d) is momentarily released prior to the next deformation upon the application of the opposite signal frame, so that the local transmittance abruptly jumps high at a frame-transition moment. For the opposite sense, there is almost no tilt (region C in Figure 4b) because the electric field is intensified near the bottom side. Thus, there is no prior release of the tilt deformation and the following deformation can occur without the transmittance shooting up. Therefore, no optical bounce at the transition from (+) to (–) frame in two-domain system. The difference between two- and one-domain systems is clearly shown by the dotted circles on the time-dependent transmittance curves (Figure 4e).

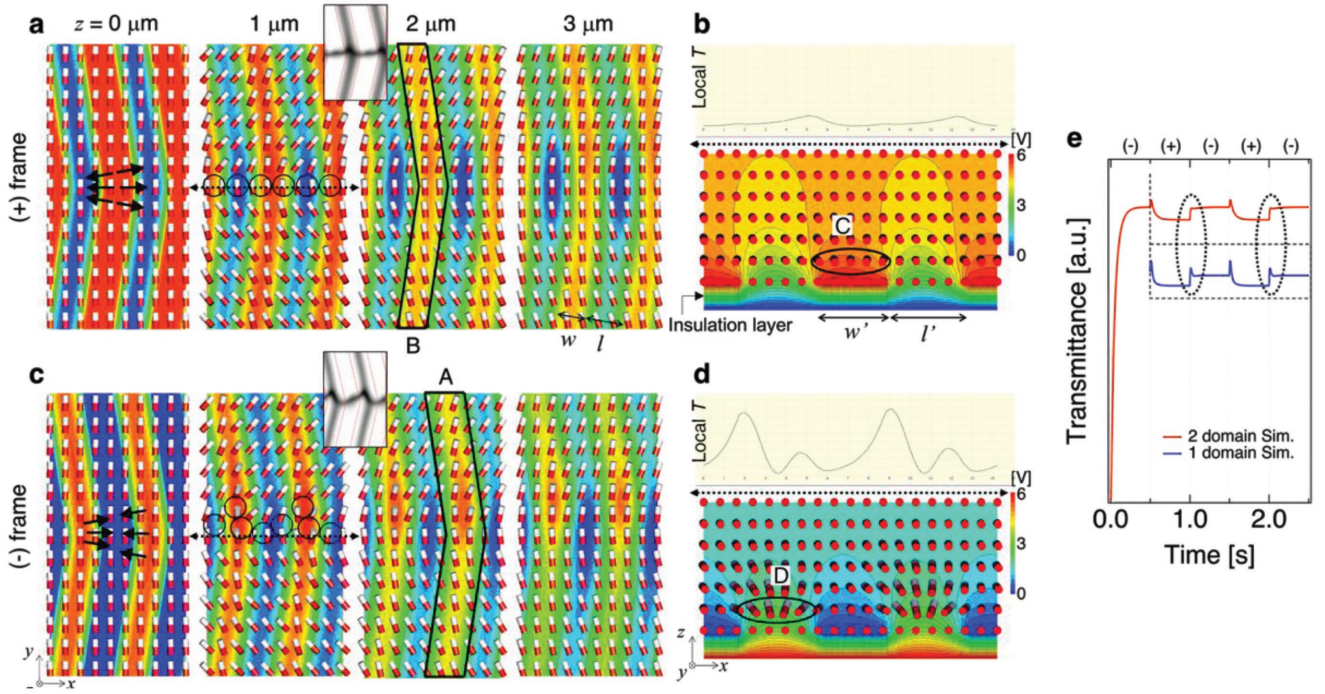

Figure 4. Detailed analysis of director fields simulated by 3D FEM. a,b) (+) and c,d) (−) frames. a,c) The director fields and electric potential distribution in the planes sliced at $z = 0$, 1, 2, and 3 μm. The black solid arrows indicate electric field direction near the domain boundary. (The boundary indicated by the black dotted arrows.) The black circles indicate no light transmitted area that matches with the 3D FEM images in the insets. b,d) The cross-sectional views along black dotted arrows in (a,c). e) Simulated time-dependent transmittance of two and one domain at $f = 1$ Hz. The difference between two and one domain is indicated by the dotted ellipses at the moment of frame transition from (+) to (−).

2.6. Elimination of Optical Flickering by the Electrode Structures with nLC

We first consider fine-patterned electrode structure to eliminate both *static* and *dynamic* image-flickering, and preliminarily, the transmittance and operation voltage V_{op} for the normal mode is calculated (**Figure 5**a). Here, we determine the transmittance difference $\Delta T/T_{avg} = 2\,(T_{s,(+)} - T_{s,(-)})/(T_{s,(+)} + T_{s,(-)})$[21] as the static image-flickering and the optical bounce $(\Delta T_{(+)} + \Delta T_{(-)})/(T_{s,(+)} + T_{s,(-)}) = ([T_{p,(+)} - T_{s,(+)}] + [T_{p,(-)} - T_{s,(-)}])/(T_{s,(+)} + T_{s,(-)})$ as the dynamic image-flickering, where subscript s, p, (+), (−), and avg denote saturated, peak, positive, negative, and averaged, respectively, in time-dependent transmittance curves. Also, we adapt physical properties of one nLC to the simulation, which is commercially used in television sets with $\Delta\varepsilon\,(\gamma_1) = -3.2$ (94 mPa s).[30]

The result shows both the transmittance and V_{op} increase as w gets reduced, and the w-dependent transmittance and V_{op} with respect to the ratio l/w are in opposite tendency, for example, at low l/w, the transmittance is kept relatively similar but V_{op} is more significantly increased in terms of w. Thus, one can optimize w and l considering both transmittance and V_{op}. Based on this idea, we simulated various electrode structures in flexoelectric mode, and the lowest transmittance difference with respect to w, l/w, and h is found (Figure 5b–d). We choose e_s (e_b) = 5 (10) pC m^{-1} for simulation because these values are not only reasonable for nematic liquid crystals[18,22,27,28] but

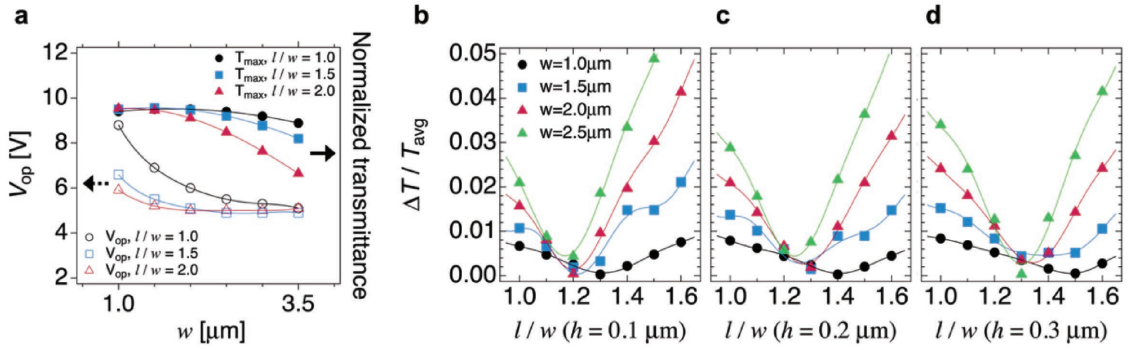

Figure 5. Electrode-structural analysis of flexoelectric FFS mode with nLC, $\Delta\varepsilon\,(\gamma_1) = -3.2$ (94 mPa s). a) Maximum transmittance and operation voltage as a function of w and l/w. b–d) The transmittance difference between frames as a function of w, l/w, and h. The flexoelectric coefficients are set by e_s (e_b) = 5 (10) pC m^{-1}.

also to have sufficient flexoelectric effect; thus, it can be minimized by the electrode-structural optimization. The minimum $\Delta T/T_{avg}$ is found depending on the electrode condition, and occurs at higher l/w as h becomes thicker.

2.7. Elimination of Optical Flickering by Optimizing Dielectric Anisotropy and Rotational Viscosity

In **Table 3** and **Figure 6**a, maximum transmittance T_{max}, transmittance difference ($\Delta T/T_{avg}$), and optical bounce $(\Delta T_{(+)} + \Delta T_{(-)})/(T_{s,(+)} + T_{s,(-)})$ of 12 cases, which show the lowest transmittance difference from Figure 5 with respect to the reference case, are summarized. Overall, the characteristics are all enhanced by the fine-patterned electrode structure toward a good electro-optic performance.

To elaborate the effect of increase of $\Delta\varepsilon$ and γ_1, we picked two cases (ii and x) and extrapolated dielectric anisotropy and rotational viscosity $\Delta\varepsilon$ (γ_1) = −8.6 (142 mPa s), which follows the linear correlation between $\Delta\varepsilon$ and γ_1,[29] for further comparison at the same structural condition. One can confirm not only the transmittance difference is eliminated in the voltage-dependent transmittance curves of the cases ii, x, ii′, and x′ (Figure 6b), but also the optical bounce disappears with the high $|\Delta\varepsilon|$ (Figure 6c–e). Moreover, the transmittance is improved and the operation voltage is reduced by high $|\Delta\varepsilon|$. In summary, the electro-optic properties can be highly enhanced as compared to the reference case: for the case ii, T_{max} by 5.3%, $\Delta T/T_{avg}$, by −76.3%, and optical bounce by −50%; the case x, T_{max} by 5.1%, $\Delta T/T_{avg}$, by −76.9%, and optical bounce by −46%; for the case ii′, T_{max} by 10.6%, $\Delta T/T_{avg}$, by −89.1%, and optical bounce by −91.8%; for the case x′, T_{max} by 10.4%, $\Delta T/T_{avg}$, by −97.3%, and optical bounce by −89.7% as shown in Table 3 and Figure 6.

2.8. Analysis on the Electrode-Structural Effect on Image-Flickering

The director fields of the reference case and the case x at the frame-transition moment are compared (**Figure 7**). At first, reducing w and l causes increase in the area of twist deformation rather than tilt deformation; thus, T_{max} increases. Second, increasing the area of twist deformation results in not only enhanced T_{max} but also less transmittance difference between frames. Third, the tilt deformation that does not contribute to T_{max} is reduced in which the electric field is intensified near bottom side as indicated by contour colors and the dark ellipses in Figure 7. As a result, although the flexoelectric polarization is spatially shifted (the local transmittance is shifted), the (spatially averaged) transmittance difference is not that significant.

2.9. Effect of Magnitude of Negative Dielectric Anisotropy and Flexoelectric Coefficients of Liquid Crystal Mixtures on Image-Flickering

To verify the effect of $|\Delta\varepsilon|$ on image-flickering, we measure and simulate with nLC1, nLC2, and nLC3 (Table 1 and **Figure 8**). We first ensure the physical parameters and cell conditions of the simulation are the same as for the experiment. The voltage-dependent transmittance curves at the normal mode in the experiment are in good agreement with that in the simulation (Figure 8a). Threshold and operation voltage are reduced as $\Delta\varepsilon$ becomes high, and the maximum transmittance also becomes high. Where applying voltage for 100% of transmittance at the flexoelectric mode in both experiment and simulation, the time-dependent transmittance curves are in close agreement

Table 3. Enhanced electro-optic properties with detailed simulation conditions.

Case	Electrode[a]			Material[b]	Electro-optic properties[c] (degree of enhancement (DOE))		
	h [μm]	w (l) [μm]	l/w	$\Delta\varepsilon$ (γ_1 [mPa s])	T_{max} (DOE [%])	$\Delta T/T_{avg}$ (DOE [%])	Optical bounce (DOE [%])
ref.	0.3	3 (4.5)	1.5	−3.2 (94)	0.312	0.0270	0.088
i	0.1	1 (1.3)	1.3	−3.2 (94)	0.334 (6.0)	0.0060 (−58.6)	0.025 (−71.5)
ii	0.1	1.5 (1.8)	1.2	−3.2 (94)	0.332 (5.3)	0.0035 (−76.3)	0.044 (−50.0)
iii	0.1	2 (2.4)	1.2	−3.2 (94)	0.327 (3.8)	0.0003 (−98.1)	0.062 (−29.0)
iv	0.1	2.5 (3)	1.2	−3.2 (94)	0.321 (1.9)	0.0016 (−88.7)	0.075 (−14.4)
v	0.2	1 (1.4)	1.4	−3.2 (94)	0.334 (5.8)	0.0064 (−56.2)	0.029 (−67.6)
vi	0.2	1.5 (1.95)	1.3	−3.2 (94)	0.332 (5.2)	0.0050 (−65.8)	0.046 (−47.5)
vii	0.2	2 (2.6)	1.3	−3.2 (94)	0.327 (3.8)	0.0032 (−78.2)	0.063 (−28.6)
viii	0.2	2.5 (3)	1.2	−3.2 (94)	0.322 (2.0)	0.0023 (−83.8)	0.075 (−15.2)
ix	0.3	1 (1.5)	1.5	−3.2 (94)	0.334 (6.0)	0.0071 (−50.7)	0.030 (−65.3)
x	0.3	1.5 (2.1)	1.4	−3.2 (94)	0.331 (5.1)	0.0034 (−76.9)	0.047 (−46.0)
xi	0.3	2 (2.6)	1.3	−3.2 (94)	0.327 (3.7)	0.0010 (−93.2)	0.063 (−28.7)
xii	0.3	2.5 (3.25)	1.3	−3.2 (94)	0.321 (1.7)	0.0034 (−81.0)	0.077 (−12.8)
ii′	0.1	1.5 (1.8)	1.2	−8.6 (142)	0.349 (10.6)	0.0030 (−89.1)	0.007 (−91.8)
x′	0.3	1.5 (2.1)	1.4	−8.6 (142)	0.348 (10.4)	0.0007 (−97.3)	0.009 (−89.7)

[a] h: insulation layer; w: electrode width; l/w: the ratio of space l to the width of electrodes; [b] $\Delta\varepsilon$ (γ_1): dielectric anisotropy (rotational viscosity); [c] T_{max}: maximum transmittance; $\Delta T/T_{avg}$: transmittance difference between signal frames.

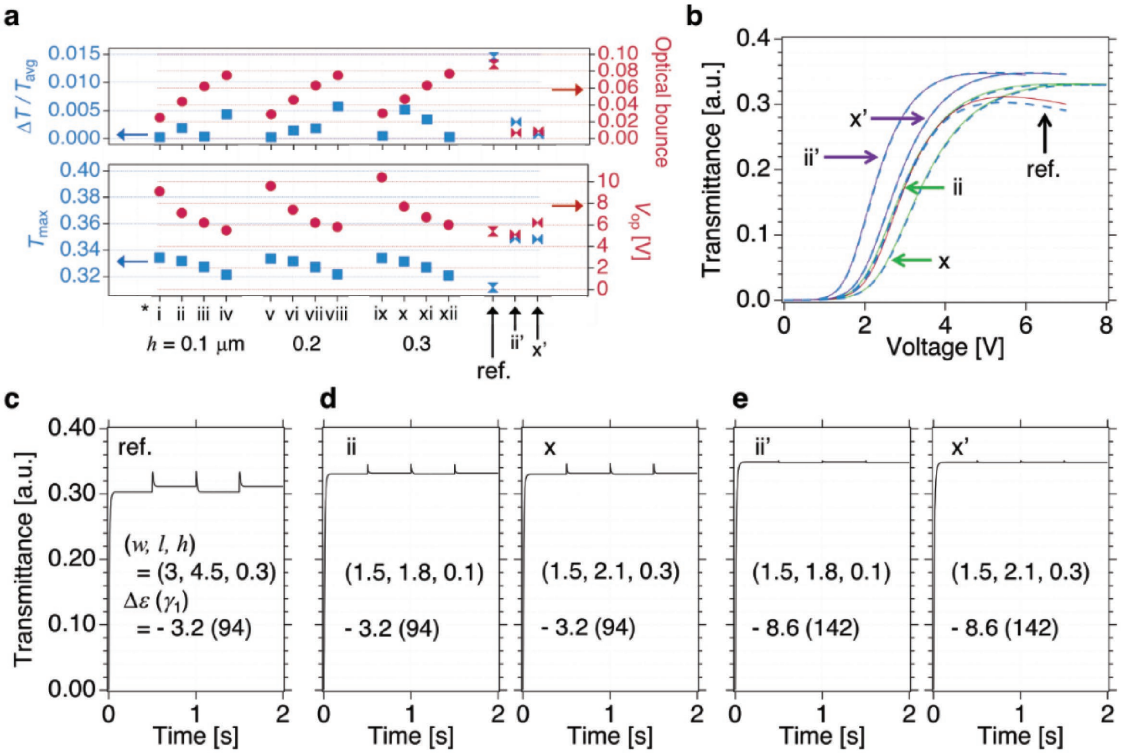

Figure 6. Enhanced electro-optic characteristics of FFS mode with fine-patterned electrodes and high magnitude of negative dielectric anisotropy. The cases ii and x: $\Delta\varepsilon$ (γ_1) = –8.6 (142 mPa s), and the cases ii′ and x′: $\Delta\varepsilon$ (γ_1) = – 3.2 (94 mPa s). a) The maximum transmittance T_{max}, operation voltage V_{op}, transmittance difference $\Delta T/T_{avg}$, and optical bounce $(\Delta T_{(+)} + \Delta T_{(-)})/(T_{s,(+)} + T_{s,(-)})$ of the reference case, and cases ii′ and x′, and the picked conditions from Figure 5 (see Table 3 for detailed conditions of 12 cases). b) Voltage-dependent transmittance, and c–e) time-dependent transmittance of the reference case, the cases ii, x, and the cases ii′, x′.

at various dielectric anisotropies and flexoelectric coefficients: nLC1, $\Delta\varepsilon$ = 2.1, e_s (e_b) = 2 (4) pC m^{-1}; nLC2, $\Delta\varepsilon$ = 3.0, e_s (e_b) = 1.7 (3.4) pC m^{-1}; and nLC3, $\Delta\varepsilon$ = 4.0, e_s (e_b) = 1 (2) pC m^{-1}. Here, the overall transmittance becomes high while the transmittance difference between frames becomes reduced because of increased $\Delta\varepsilon$ and lowered e_s (e_b): the nLC3 has higher $|\Delta\varepsilon|$ and lower e_s (e_b) than those of nLC1. Additional simulated results with the same e_s (e_b) for all nLCs show different behaviors from the experimental results (Figure S2, Supporting Information).

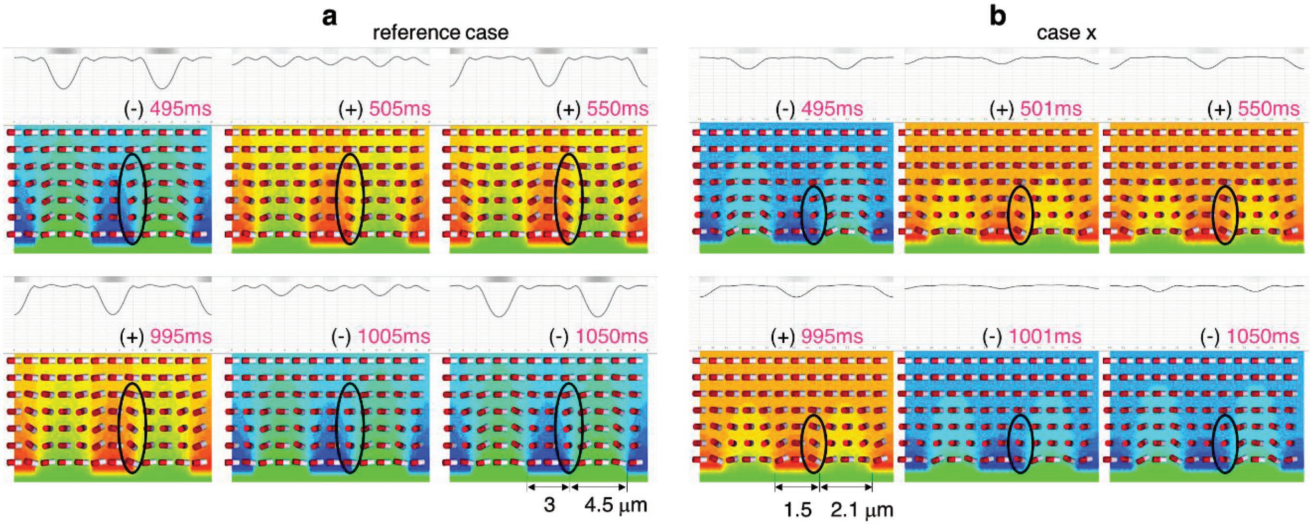

Figure 7. Director field analysis for the effect of the fine-patterned electrode. Tracking of local transmittance change at the transition moment between signal frames of a) reference case and b) case x (in the dark ellipses). In the case x, the optical bounce is less than that in the reference case.

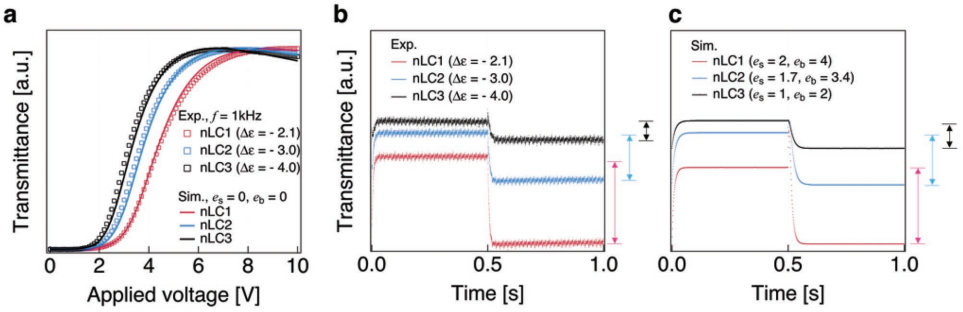

Figure 8. Electro-optic measurement and simulation results with various magnitude of negative dielectric anisotropy of liquid crystal mixtures and their flexoelectric coefficients. a) Measured and simulated voltage-dependent transmittance of nLC1, 2, and 3 from Table 1. b) Measured time-dependent transmittance curves and c) simulated time-dependent transmittance curves of nLC1, 2, and 3. The black, blue, and red arrows indicate the transmittance difference between the signal frames.

3. Discussion

Although the FEM simulation method has been well known for LCD technology to predict quite high agreement with the experimental results, not only in the academic but also in the industrial field, the results in Figures 5 and 6 would be limited to the particular physical parameters including flexoelectric coefficients we choose in this work. However, the demonstration of flexoelectric behavior with pLC in Figures 2–4 and with nLC in Figure 8 is in quite close agreement between experiments and simulations. Based on this fact, we believe the claimed results with superior performance we calculated and predicted can be reasonably addressed.

From the equations of flexoelectric coefficients (see Section 2.2), other than the two variables (the molecular dipole moment μ and the molecular number density N), one may approach to adjust elastic constants K_{11} (K_{33}), the kink angle β, or the molecular aspect ratio a/b (b/a). In our approach with nLCs, the elastic constants are almost fixed. And either the kink angle or molecular aspect ratio would not vary for three nLCs because the number of possible conformations of the single compounds would not be very different from each other as well as that of the aspect ratio (see Figure 1).

The difference of flexoelectric coefficients between the compound **1** and **3** can be similarly considered as those between well-known liquid crystal molecules PCH5 and 5CB (Figure S1, Supporting Information). Their flexoelectric coefficients measured with elastic constants, PCH5: $(e_s + e_b)/K_{22} \approx 1.66$ C N^{-1} m^{-1} and $(e_s - e_b)/K_{33} \approx 0.12$ C N^{-1} m^{-1}; 5CB: $(e_s + e_b)/K_{22} \approx 2.40$ C N^{-1} m^{-1} and $(e_s - e_b)/K_{33} \approx 1.08$ C N^{-1} m^{-1}. The estimation of e_s (e_b) with previously measured elastic constants turns into PCH5: e_s (e_b) ≈ 0.131 (0.125) C m^{-1}; 5CB: e_s (e_b) ≈ 0.454 (0.346) C m^{-1}, which implies higher flexoelectric coefficients with rigid molecular compound regardless of the dipole moments along the cyano polar group (see Figure S1 and Table S1, Supporting Information).

The time-dependent transmittance curves in Figure 8 show less dynamic flickering than the results with similar dielectric anisotropy in Figure 6 even though the electrodes are not fine-patterned. The main reason we can discuss here can be the low-flexoelectric coefficients. The low-flexoelectric coefficients would not give rise to high dynamic flickering but the transmittance difference is still shown because the asymmetry of electric fields exists with the nonsymmetrized, non-fine-patterned electrode condition. Also, the result in Figure 8 demonstrates the effect of the liquid crystal mixture having higher $|\Delta\varepsilon|$ and lower flexoelectric coefficients. In the liquid crystal mixture, there are more other compounds than the ones introduced here.

4. Conclusion

We have demonstrated low-frequency driving liquid crystal displays with multiple functionalities including power-saving mode and superior electro-optic performance. At low-frequency driving, flexoelectric effect arises owing to the coupling between electric polarization and director deformation on liquid crystal materials. The image-flickering caused by the flexoelectric effect becomes apparent even to human eye perception owing to the spatial shift of flexoelectric polarization and momentary relaxation of it (tilt deformation). From a perspective of liquid crystal material engineering, the image-flickering can be suppressed by high magnitude of negative dielectric anisotropy as it can restrain the tilt deformation of liquid crystal director under applied electric signal (thereby, enhancing the twist deformation that contributes to higher optical transmittance). This method contributes to both extremely high transmittance and stable images during the frame-transition. However, increasing molecular dipole moment in a mixture gives rise to increase not only dielectric anisotropy but also flexoelectric coefficients because both are proportional to the dipole moment. Here, flexible molecules, for example, containing a cyclohexane instead of a benzene ring, in a mixture can reduce flexoelectric coefficients regardless of the molecular dipole moment. In this way, liquid crystals can be highly functionalized for superior performance and low power consumption liquid crystal displays. Also, by optimizing fine-patterned electrode structure, to reduce the electrode width and space between electrodes with symmetrized electric field formation give rise to the highly intensified electric field near the electrodes, hence contributing to reduction in image-flickering. We practically dealt with the issue from an engineering perspective with specific and sufficient results and clearly demonstrated a suitable design for realization of power saving displays with ever superior electro-optic performance. We believe these results can suggest a new way to develop multifunctional liquid crystal materials and device structures for high-performance and power-saving mode liquid crystal displays.

5. Experimental Section

Cell Preparation: Both pLC and nLC cells for experiments of FFS mode were prepared; detailed information is given in Table 1. On one glass substrate side, three layers were sputter-coated: one transparent ITO layer, an insulation layer (SiO_2), and the other transparent ITO layer. And then the top ITO layer was patterned by photolithography. Homogeneous alignment layers (PI-2555, Nissan Chemical Industries Ltd.) were spin-coated on both the electrode substrate and the other bare glass substrate, and rubbed with an angle α to the long direction of electrodes. The two substrates were then assembled while maintaining the cell gap d by ball spacers, and nematic liquid crystal mixtures were injected.

Image Acquisition by POM and High-Speed Camera: The POM images were taken by using a high-speed camera (Phantom v211, Vision Research Inc.) with 200 frames per second (fps) and the exposure time <5 ms in which cell is sandwiched by two crossed polarizers. Thus, series of the frames under positive and negative polarities of the applied electric fields were systematically acquired. By image-processing, the local transmittance in the spatial region of interest, which is indicated by the black arrow in Figure 2c, can be plotted.

Electro-Optic Measurement: The electro-optic measurement was done by an automated acquisition system performing the voltage application and photodetection: voltages were applied and swung between (+) and (–) frames using a function generator (DS345, Stanford Research Systems Inc.) and static and dynamic responses were measured using combination of a tungsten-halogen light source (Radiometric Fiber Optic Illuminator 77501, Oriel Instruments) filtered by monochromatic wave λ = 554 nm and a 1° narrow-angle luminance probe (J6523, Tektronix Inc.). The driving frequency was applied by f = 1 kHz at the normal mode and f = 1 Hz at the flexoelectric mode.

Supporting Information

Supporting Information is available from the Wiley Online Library or from the author.

Acknowledgements

This research was supported partially by the Basic Science Laboratory Research Program [2014R1A4A1008140] through the National Research Foundation of Korea (NRF) funded by the Ministry of Science, ICT & Future Planning and partially by the Basic Science Research Program [2016R1D1A1B01007189] through the National Research Foundation of Korea (NRF) funded by the Ministry of Education. D.-K.Y. acknowledges the support from BOE Co. M.K. and S.H.L. conceived and designed the work; M.K. and H.S.J. performed experiments; M.K and H.G.H. performed FEM simulations; M.K. and Y.-H.S. performed MOPAC simulation; M.K., S.H.L., and P.J.B. contributed to the writing and proofreading of the manuscript. The authors gratefully acknowledge the critical reading and correction of the manuscript by Prof. Francesca Serra.

Conflict of Interest

The authors declare no conflict of interest.

Keywords

electro-optical materials, flexoelectric effect, image-flickering, liquid crystals, liquid crystal displays

Received: January 8, 2018
Revised: February 4, 2018
Published online: March 25, 2018

[1] International Energy Agency, Organisation for Economic Co-operation and Development, *Gadgets and Gigawatts : Policies for Energy Efficient Electronics*, IEA, **2009**, https://www.iea.org/publications/freepublications/publication/gigawatts2009.pdf.
[2] I. Hwang, C. W. Park, S. C. Kang, D. S. Sakong, *SID Symp. Dig. Tech. Pap.* **2001**, *32*, 492.
[3] C. Mantel, N. Burini, E. Nadernejad, J. Korhonen, S. Forchhammer, J. M. Pedersen, *J. Disp. Technol.* **2013**, *9*, 933.
[4] S. H. Lee, S. L. Lee, H. Y. Kim, *Appl. Phys. Lett.* **1998**, *73*, 2881.
[5] M. Oh-e, K. Kondo, *Appl. Phys. Lett.* **1995**, *67*, 3895.
[6] D.-K. Yang, S.-T. Wu, *Fundamentals of Liquid Crystal Devices*, Wiley, New York **2015**.
[7] T. Tsuruma, Y. Goto, A. Higashi, M. Watanabe, H. Yamaguchi, T. Tomooka, H. Kikkawa, in *31st International Display Research Conference 2011 (EuroDisplay 2011)*, Arcachon, France, Curran Associates, Inc., Red Hook, NY **2011**, pp. 15–18.
[8] R. Hatsumi, S. Fukai, Y. Kubota, A. Yamashita, M. Jikumaru, H. Baba, K. Moriya, D. Kubota, K. Kusunoki, Y. Hirakata, J. Koyama, S. Yamazaki, Y. Chubachi, C. Fujiwara, *J. Soc. Inf. Disp.* **2013**, *21*, 442.
[9] H. Chen, F. Peng, M. Hu, S.-T. Wu, *Liq. Cryst.* **2015**, *42*, 1730.
[10] D.-J. Lee, G.-Y. Shim, J.-C. Choi, J.-S. Park, J.-H. Lee, J.-H. Baek, H. C. Choi, Y. M. Ha, A. Ranjkesh, H.-R. Kim, *Opt. Express* **2015**, *23*, 34055.
[11] J.-W. Kim, T.-H. Choi, T.-H. Yoon, E.-J. Choi, J.-H. Lee, *Opt. Express* **2014**, *22*, 30586.
[12] I. H. Jeong, I. W. Jang, D. H. Kim, J. S. Han, B. V. Kumar, S. H. Lee, S. H. Ahn, S. H. Cho, C. Yi, *SID Symp. Dig. Tech. Pap.* **2013**, *44*, 1368.
[13] H. S. Choi, J. H. Kim, H. G. Ham, Y. J. Lim, J. M. Lee, H. S. Jin, R. Manda, M. S. Kim, D.-K. Yang, S. H. Lee, *SID Symp. Dig. Tech. Pap.* **2016**, *47*, 1610.
[14] S.-W. Oh, J.-H. Park, J.-H. Lee, T.-H. Yoon, *Opt. Express* **2015**, *23*, 24013.
[15] R. B. Meyer, *Phys. Rev. Lett.* **1969**, *22*, 918.
[16] W. Helfreich, *Z. Naturforsch., A: Phys. Sci.* **1971**, *26*, 833.
[17] J. Prost, P. S. Pershan, *J. Appl. Phys.* **1976**, *47*, 2298.
[18] A. Buka, N. Eber, *Flexoelectricity in Liquid Crystals: Theory, Experiments and Applications*, World Scientific, Singapore **2012**.
[19] M. S. Kim, P. J. Bos, D.-W. Kim, D.-K. Yang, J. H. Lee, S. H. Lee, *Sci. Rep.* **2016**, *6*, 35254.
[20] J. Harden, B. Mbanga, N. Eber, K. Fodor-Csorba, S. Sprunt, J. T. Gleeson, A. Jákli, *Phys. Rev. Lett.* **2006**, *97*, 157802.
[21] M. S. Kim, P. J. Bos, D.-W. Kim, C.-M. Keum, D.-K. Yang, H. G. Ham, K.-U. Jeong, J. H. Lee, S. H. Lee, *Opt. Express* **2016**, *24*, 29568.
[22] M. S. Kim, H. G. Ham, H.-S. Choi, P. J. Bos, D.-K. Yang, J. H. Lee, S. H. Lee, *Opt. Express* **2017**, *25*, 5962.
[23] H. J. Yun, M. H. Jo, I. W. Jang, S. H. Lee, S. H. Ahn, H. J. Hur, *Liq. Cryst.* **2012**, *39*, 1141.
[24] I. H. Yu, I. S. Song, J. Y. Lee, S. H. Lee, *J. Phys. D: Appl. Phys.* **2006**, *39*, 2367.
[25] J. J. P. Stewart, *J. Comput.-Aided Mol. Des.* **1990**, *4*, 1.
[26] D. Pauluth, K. Tarumi, *J. Soc. Inf. Disp.* **2005**, *13*, 693.
[27] A. Ferrarini, C. Greco, G. R. Luckhurst, *J. Mater. Chem.* **2007**, *17*, 1039.
[28] H. Lee, H. Kim, J. Kim, J. H. Lee, *J. Phys. D: Appl. Phys.* **2016**, *49*, 075501.
[29] H. Chen, M. Hu, F. Peng, J. Li, Z. An, S.-T. Wu, *Opt. Mater. Express* **2015**, *5*, 655.
[30] M. Bremer, M. Klasen-Memmer, D. Pauluth, K. Tarumi, *J. Soc. Inf. Disp.* **2006**, *14*, 517.